bioRxiv preprint doi: https://doi.org/10.1101/2022.09.03.506477; this version posted September 5, 2022. The copyright holder for this preprint (which was not certified by peer review) is the author/funder. All rights reserved. No reuse allowed without permission.

Structures and membrane interactions of native serotonin transporter in complexes with psychostimulants

Dongxue Yang[1,4], Zhiyu Zhao[3], Emad Tajkhorshid[3], and Eric Gouaux[1,2]

1. Vollum Institute, Oregon Health & Science University, Portland, Oregon 97239, USA.
2. Howard Hughes Medical Institute, Oregon Health & Science University, Portland, Oregon 97239, USA.
3. Department of Biochemistry, NIH Center for Macromolecular Modeling and Bioinformatics, Beckman Institute for Advanced Science and Technology, and Center for Biophysics and Quantitative Biology, University of Illinois at Urbana-Champaign, Urbana, IL, USA.
4. Present address: Department of Urology, Institute of Urology (Laboratory of Reconstructive Urology), West China Hospital, Sichuan University, Chengdu, Sichuan, China.

Correspondence to Eric Gouaux: gouauxe@ohsu.edu

bioRxiv preprint doi: https://doi.org/10.1101/2022.09.03.506477; this version posted September 5, 2022. The copyright holder for this preprint (which was not certified by peer review) is the author/funder. All rights reserved. No reuse allowed without permission.

SUMMARY

The serotonin transporter (SERT) is a member of the SLC6 neurotransmitter transporter family that mediates serotonin reuptake at presynaptic nerve terminals. SERT is the target of both therapeutic antidepressant drugs and illicit psychostimulant substances such as cocaine and methamphetamines, which are small molecules that perturb normal serotonergic transmission by interfering with serotonin transport. Despite decades of studies, the oligomerization state of native SERT (nSERT) and its interactions with potential proteins remain unresolved. Here we develop methods to isolate nSERT from porcine brain, utilize fluorescence-detection size-exclusion chromatography to investigate the nSERT oligomerization state, and report single-particle cryo-electron microscopy structures of nSERT in complexes with methamphetamine and cocaine, providing structural insights into psychostimulant recognition and accompanying nSERT conformations. Methamphetamine and cocaine both bind to SERT central site, stabilizing the transporter in outward and outward-occluded conformations, respectively. We also identify densities attributable to multiple cholesterol molecules, as well as to a potential polyunsaturated lipid bound to SERT allosteric site. Our study establishes that nSERT is best described as a monomeric entity, isolated without interacting proteins, and is ensconced by multiple cholesterol and lipid molecules.

bioRxiv preprint doi: https://doi.org/10.1101/2022.09.03.506477; this version posted September 5, 2022. The copyright holder for this preprint (which was not certified by peer review) is the author/funder. All rights reserved. No reuse allowed without permission.

Introduction

Serotonin is a neurotransmitter that modulates multiple fundamental brain functions that include memory, learning, sleep, pain, mood, and appetite[1]. The serotonin transporter (SERT) removes serotonin from synaptic, perisynaptic and extracellular regions by harnessing the energy from sodium and chloride transmembrane gradients, diminishing local serotonin concentrations and thus terminating serotonergic neurotransmission[2]. Congruent with the crucial roles of serotonergic signaling in neurophysiology, dysfunction of SERT has profound consequences associated with neurological disease and disorders, including Parkinson's disease, seizures, depression, epilepsy, and attention deficit hyperactivity disorder[2,3].

SERT is a member of the large neurotransmitter transporter family, also known as neurotransmitter sodium symporters (NSSs). Additional members of the NSS family include transporters for norepinephrine (NET), dopamine (DAT), glycine (GlyT1 and GlyT2), and γ-aminobutyric acid (GAT), as well as for betaine and creatine[2]. The NSSs are made up of 12 transmembrane helices organized topologically into two inverted repeats that, in turn comprise a conserved three-dimensional fold known as the LeuT fold[4]. Substrate transport by NSSs is described by an alternating access mechanism[5] in which the substrate is translocated from extracellular to intracellular spaces[6-12].

SERT is a longstanding pharmacological target for antidepressant drugs[13], as well as for psychostimulants such as cocaine, amphetamine, and methamphetamine[14]. The therapeutic utility of the drugs that act on SERT, including the selective serotonin reuptake inhibitors (SSRIs), is a consequence of their specific action on SERT resulting in their relative lack of inhibition of the closely related DAT and NET transporters. By contrast, illicit, psychoactive drugs such as cocaine and amphetamines also inhibit DAT and NET, and as a consequence, they have pleotropic effects on the neurotransmitter reuptake systems, thus explaining their psychoactive and deleterious effects on neurophysiology and behavior[13]. The potent and widely abused psychostimulants amphetamine, methamphetamine, and cocaine as well as synthetic cocaine derivatives, competitively inhibit the transport of neurotransmitters and lock the transporter in a

bioRxiv preprint doi: https://doi.org/10.1101/2022.09.03.506477; this version posted September 5, 2022. The copyright holder for this preprint (which was not certified by peer review) is the author/funder. All rights reserved. No reuse allowed without permission.

transport inactive conformation, resulting in prolonged neurotransmission in the brain or promoting neurotransmitter efflux into the synaptic space[2]. The primary mechanism of addiction is thought to be increased monoamine signaling in the central nervous system. The X-ray structures of a transport-inactive *Drosophila melanogaster* DAT (dDAT) NSS transporter in complex with cocaine, amphetamine, or methamphetamine have revealed that elicit psychostimulants bind at the central substrate-binding site to the transporter, consistent with their competitive inhibition[15].

Multiple studies suggest that SERT interacts with a variety of intracellular scaffolding, cytoskeletal, anchoring, and signaling proteins. A prominent example includes syntaxin1A, a vesicle fusion SNARE protein, which has been shown to interact directly with the amino terminus of SERT and regulate its cell surface expression level[16]. By contrast, a neuronal nitric-oxide synthase (nNOS) that has a postsynaptic density of 95/discs-large/zona occludens (PDZ) domain interacts with the carboxy terminus of SERT, reducing its surface expression level and serotonin uptake capacity[17]. Hydrogen peroxide-inducible clone-5 (Hic-5) is a scaffolding protein that has been linked to SERT to aid in its internalization[18]. While protein-protein interactions regulate SERT function and subcellular distribution, the extent to which they form stable complexes for biochemical isolation is not well understood.

SERT also has cytoplasmic domains with numerous consensus sites for post-translational modification by protein kinases, phosphatases, and other interacting proteins that modulate its transporter function and cellular distribution[19]. SERT possesses two consensus sites for *N*-linked glycosylation within the extracellular loop 2 (EL2; Asn208, Asn217) whose glycosylation is related to cell-surface expression of the transporter[20]. Protein kinase C (PKC) phosphorylates the cytoplasmic N- and C-terminal regions of SERT. Although no specific sites have been identified for this modification, PKC phosphorylation of SERT decreases the overall transport rate by promoting SERT redistribution from the plasma membrane to intracellular compartments[21]. Modification of SERT by the cGMP-stimulated protein kinase G (PKG) occurs on threonine residues, such as Thr276 (ref. 22). Interestingly, Thr276 is

bioRxiv preprint doi: https://doi.org/10.1101/2022.09.03.506477; this version posted September 5, 2022. The copyright holder for this preprint (which was not certified by peer review) is the author/funder. All rights reserved. No reuse allowed without permission.

95 located on the intracellular end of TM5 and is only partially exposed, thus providing
96 insight into how its modification is coupled to the stabilization of specific
97 conformational states[22]. Calcium/calmodulin-dependent protein kinase II (CaMKII)
98 activity has been reported to regulate the electrophysiological properties of the
99 transporter by modulating its interaction with syntaxin1A[16]. Tyr phosphorylation has
100 also been shown to regulate SERT function, and 5-HT uptake capacity into platelets,
101 which is positively correlated with Src-mediated Tyr phosphorylation[23]. Protein kinase
102 A (PKA) mediated *in vitro* phosphorylation has also been reported for the isolated C-
103 and N-terminal domains of SERT expressed as fusion proteins[21]. Although major efforts
104 have been directed toward understanding the role of phosphorylation of SERT, more
105 work is needed to understand the molecular basis of transporter regulation by
106 phosphorylation.

107 The oligomerization states of SERT and related NSSs have been studied in the
108 contexts of the plasma and organellar membranes[24,25]. Radiation inactivation and
109 mutagenesis studies provided the first glimpse into SERT oligomerization[26].
110 Experiments with cross-linkers additionally suggested that rat SERT can form dimers
111 and tetramers to varying degrees[27]. Subsequent studies investigating the
112 oligomerization state of NSSs have employed co-immunoprecipitation[28-30], Förster
113 resonance energy transfer (FRET) measurements[30-36], and fluorescence lifetime
114 imaging microscopy[35]. Many of these studies were interpreted with an oligomerization
115 model where the transporters form a variety of quaternary arrangements, ranging from
116 monomers to multimers, differing to some extent depending on the specific NSSs[33,35,37-
117 39]. Membrane components such as phosphatidylinositol 4,5-bisphosphate (PIP2) and
118 other lipids also have been implicated in the formation of NSS oligomers[40,41],
119 presumably via lipid interactions to the transmembrane part of the protein, while
120 psychostimulants such as methamphetamine and amphetamine have been shown to
121 influence transporter oligomerization through an unknown mechanism[34,42,43].

122 Despite extensive experimental data from a broad range of biochemical,
123 biophysical and computational studies[44,45] that have been interpreted in terms of SERT

bioRxiv preprint doi: https://doi.org/10.1101/2022.09.03.506477; this version posted September 5, 2022. The copyright holder for this preprint (which was not certified by peer review) is the author/funder. All rights reserved. No reuse allowed without permission.

oligomers, there has been no direct evidence for its oligomerization state based on the purified transporter isolated from a native source. Here, we develop methods to extract nSERT from porcine brain tissue using the high-affinity 15B8 Fab, in the presence of methamphetamine and cocaine, respectively, allowing us to study the purified complex using fluorescence-detection size-exclusion chromatography (FSEC). We then carry out high-resolution, single-particle cryo-electron microscopy (cryo-EM) reconstructions, together with computational studies, to probe the conformation of psychostimulant-bound transporter and its interaction with lipids of a native cell membrane.

Results

Purification and cryo-EM of the native transporter

To isolate nSERT, we exploited the 15B8 Fab[10], an antibody fragment that binds to a tertiary epitope of human SERT (hSERT), yet does not hinder the binding of ligands or the transport activity. We hypothesized that because porcine SERT and hSERT are closely related in amino acid sequence, the 15B8 Fab would also bind to porcine SERT and could serve as a powerful tool for immunoaffinity isolation of the transporter. We thus engineered the 15B8 Fab with a carboxy terminal mCherry fluorophore and an affinity tag (Fig. 1a).

To isolate nSERT from porcine brain membranes, we next explored a wide range of membrane protein solubilization conditions, aiming to extract the transporter under the mildest conditions while retaining as much surrounding native lipid as possible. We thus first attempted solubilization in the presence of styrene-maleic acid (SMA) co-polymer[46] or recently developed amphipols[47]. Unfortunately, neither yielded a measurable amount of nSERT as shown by FSEC analysis (Fig. 1b). We then examined the classical non ionic detergents, n-dodecyl-β-D-maltoside (DDM) together with cholesterol hemisuccinate (CHS) or digitonin, based on their utility in extraction of recombinant SERT[10]. Surprisingly, a peak for the SERT-15B8 Fab-mCherry complex was only observed for the DDM/CHS mixture (Fig. 1b). We therefore utilized

bioRxiv preprint doi: https://doi.org/10.1101/2022.09.03.506477; this version posted September 5, 2022. The copyright holder for this preprint (which was not certified by peer review) is the author/funder. All rights reserved. No reuse allowed without permission.

DDM/CHS in all subsequent studies. To isolate the nSERT from porcine brain tissue, we incubated the solubilized membranes with an excess of the 15B8 Fab-mCherry protein, as well as with saturating concentrations of either methamphetamine or cocaine. The transporter was purified by affinity chromatography, followed by FSEC and the manual collection of fractions (Fig. 1c). Analysis of the isolated material by western blot revealed a band migrating with an apparent mass of 75kDa (Fig. 1d), consistent with the estimated mass of nSERT. The well-resolved and symmetrical FSEC peak indicated that the purified nSERT 15B8 Fab-mCherry complex was monodisperse. The elution volume with FSEC of nSERT 15B8 Fab complex was consistent with the recombinant ts2-15B8 complex (Fig. 1c), indicating the purified nSERT was a monomer.

To explore the function of nSERT, we carried out saturation binding experiments using the high-affinity SSRI [^{3}H]paroxetine and determined a dissociation constant (K_d) of 6.5 ± 1.3 nM (Fig. 1e), consistent with previous measurements[8]. To characterize methamphetamine and cocaine binding with nSERT, we next performed competition experiments, similarly employing [^{3}H]paroxetine, and measured inhibitory constants (K_i) of 199 ± 103.4 µM (Fig. 1f) and 179 ± 68 nM (Fig. 1g), respectively, thus indicating that both methamphetamine and cocaine compete for [^{3}H]paroxetine binding, consistent with the psychostimulants binding to the central site. The potency of methamphetamine and cocaine on nSERT differs by a factor of ~1,000, in accord with previous studies, whereas the two ligands are equally potent on DAT[48], underscoring the differences in residue composition and plasticity of the central binding pockets of SERT and DAT. Taken together, the ligand binding data illustrate that our purification method yields native transporter fully active in ligand binding.

From one pig brain we obtained ~20 µg of purified protein in a volume of 200 µL, which was sufficient for visualizing particles on continuous carbon-coated grids under cryogenic conditions. We then collected single-particle cryo-EM data sets and carried out reconstructions of the methamphetamine- and cocaine-bound SERT complexes, obtaining density maps that extended to approximately 2.9 and 3.3 Å

bioRxiv preprint doi: https://doi.org/10.1101/2022.09.03.506477; this version posted September 5, 2022. The copyright holder for this preprint (which was not certified by peer review) is the author/funder. All rights reserved. No reuse allowed without permission.

resolutions, respectively (Supplementary Fig. 1-5 and Supplementary Table 1, Supplemental Fig. 6a-b). Thorough 2D and 3D classifications yielded a single class for each data set in which nSERT is found as a monomeric entity, with no evidence of dimers or higher ordered oligomers (Supplementary Fig. 1-2), consistent with the molecular size of SERT estimated by FSEC. Overall, the density maps are of sufficient quality to assign most of the amino acid side chains, identify additional non-protein density within the central binding site for bound ligands, and indicate the presence of bound CHS molecules surrounding the transporter transmembrane domains (Fig. 2).

Psychostimulant occupancy of the central site

Methamphetamine binds to the central site of the nSERT complex, adopting a similar binding pose to that observed in DAT[15], lodged between the aromatic groups of Tyr213 and Tyr132. The amino groups of methamphetamine interact with Ser475 and form hydrogen bonds with the carboxylate of Asp135, and the main chain carbonyl of Phe372, as seen with the hydrogen bonds formed between the amino group of methamphetamine, and the equivalent Asp46 residue, and Phe319 residue in DAT[15] (PDB code: 4XP6). The side chain of Phe378 forms edge-to-face aromatic interactions with the phenyl group of methamphetamine (Fig. 3a, Supplementary Fig. 6c). Comparison of the positions of TM1, TM6, and the extracellular gate to the equivalent elements of serotonin-bound, outward-open SERT complex[49] (Protein Data Bank (PDB) code: 7LIA, RMSD: 0.606 Å), indicates that SERT-15B8 Fab-methamphetamine complex adopts an outward-open conformation (Fig. 3b, Supplementary Fig. 6d), which is consistent with previous structural studies of dDAT in complex with methamphetamine[15].

The structure of the SERT-cocaine complex displays an outward-occluded conformation, with cocaine occupying the entire central binding pocket with an overall similar pose to the dDAT-cocaine complex[15]. The nearly complete filling of the volume of the central site by cocaine perhaps accounts for the higher affinity of SERT for cocaine compared with methamphetamine, reminiscent of how increasing the volume of serotonin via methylated analogs can enhance ligand binding[49]. The benzoyl moiety

bioRxiv preprint doi: https://doi.org/10.1101/2022.09.03.506477; this version posted September 5, 2022. The copyright holder for this preprint (which was not certified by peer review) is the author/funder. All rights reserved. No reuse allowed without permission.

of cocaine is accommodated between TM3 and TM8, where it forms van der Waals interactions with Ile209, Tyr213, Phe378, and Thr476. The methyl ester group protrudes into the base of the extracellular vestibule and the tropane rings are bordered by Tyr132, Ala133, Asp135, Phe372, and Ser475. Interestingly, the side chain of Phe372 undergoes substantial displacement and moves further into the central site than seen in the dDAT complex[15]. This reorganization translates into the closure of the inner gate from the extracellular side, blocking the release of cocaine from the central site and ultimately occluding the binding pocket, a conformation that was not seen in the cocaine-bound dDAT structure (Fig. 3c, Supplementary Fig. 6e). The overall structure of SERT-15B8 Fab-cocaine complex is similar to 5-HT bound recombinant hSERT in its outward open structure (PDB code: 7LIA, RMSD: 0.623), except for the orientation of Phe372. Because the rotation of Phe372 closes the extracellular gate, we define the conformation of the SERT-15B8 Fab-cocaine complex as an outward-occluded state (Fig. 3d, Supplementary Fig.6f).

Taken together, the structures of SERT in complexes with methamphetamine and cocaine show how the shape, chemical composition, and plasticity of the binding site enables the transporter to recognize ligands of different shapes and sizes. The distinct orientations of Phe372 in the cocaine-bound nSERT and recombinant dDAT structures emphasize the role of the central site residues in defining ligand binding affinity, which can be expanded to understanding variations in the pharmacological profiles between biogenic amine transporters.

CHS sites surround the TMD

SERT is an integral membrane protein embedded in a complex neuronal membrane composed of phospholipids, sphingolipids, and cholesterol[50]. SERT[50-52], NET[53,54], DAT[55-57], and GlyT[58,59], as well as some excitatory amino acid transporters[60] associate with cholesterol in brain tissues or in transfected cell lines. Cholesterol is implicated in a variety of biological processes, including membrane protein organization and compartmentalization within the membrane. It is also known to play a key indirect role in modulating neurotransmission via its effects on the activities of

bioRxiv preprint doi: https://doi.org/10.1101/2022.09.03.506477; this version posted September 5, 2022. The copyright holder for this preprint (which was not certified by peer review) is the author/funder. All rights reserved. No reuse allowed without permission.

DAT[61] and SERT[50]. Indeed, depletion of cholesterol from membranes affects the function of neurotransmitter transporters[61,62]. Previous molecular dynamics (MD) studies revealed six potential cholesterol binding sites in SERT, defined as CHOL1-6[63]. Bound CHOL has been observed at the CHOL1 binding site in dDAT structures[15]. The cholesterol analog, cholesteryl hemisuccinate (CHS), has been found to bind at the CHOL2 binding site in dDAT[15,64], as well as to hSERT[10], and CHS has also been observed at the CHOL3 binding site in hSERT[8]. In investigating the interactions of CHOL with nSERT, we carefully examined the density maps of methamphetamine- and cocaine-bound SERT complexes, and the quality of the density maps enabled the identification of CHS at the CHOL1 and CHOL2 binding sites in both of the structures (Fig. 4a-b, d-e), consistent with previous observations.

We also identified a non-protein density in the allosteric site for both complexes (Fig. 2), a binding site for a broad spectrum of ligands[8,49,65] (Supplementary Fig. 6g-i). The overall shape of the density resembles a lipid molecule. Because the local resolutions of the density maps within the allosteric site are not sufficient for unambiguous molecular identification, we used molecular dynamics (MD) simulations to examine the binding of the most abundant lipid molecules, steroids, or fatty acids to the allosteric site. We performed all-atom MD simulations of the cocaine-SERT complex with the allosteric site occupied by either docosahexaenoic acid (DHA), in charged or neutral forms (DHA^- or DHA^0, respectively), CHOL, or CHS, in triplicate for each lipid species. In all three independent simulations, DHA^- remained bound at the site (center-of-mass displacement ≤ 3 Å), whereas in all simulations with neutral DHA^0, CHOL, or CHS, the ligand unbinds from its binding site within nanoseconds, as highlighted by large center-of-mass displacements (> 5 Å) (Fig. 4g, Supplementary Fig. 7a). We further performed bias-exchange umbrella sampling simulations to calculate binding free energy profiles for DHA^- and CHOL, verifying preferential binding of DHA^- to the allosteric site, whereas CHOL binding to this site appears to be accompanied with a large penalty in free energy (Fig. 4h, Supplementary Fig. 7b-c). This suggests the allosteric site is not a preferred cholesterol-binding site and instead

bioRxiv preprint doi: https://doi.org/10.1101/2022.09.03.506477; this version posted September 5, 2022. The copyright holder for this preprint (which was not certified by peer review) is the author/funder. All rights reserved. No reuse allowed without permission.

accommodates fatty acid binding. We thus fit DHA into this site (Fig. 4c and f). The DHA molecule adopts a curled orientation, with the flexible fatty acid tail protruding between TM11 and TM12, and the carboxylate group extending into the extracellular vestibule (Fig. 4c and f). The role of lipid binding within the allosteric site awaits further elucidation.

Discussion

Despite indirect experimental results suggesting that monoamine transporters might form oligomeric quaternary complexes[25], there is no direct determination of the oligomerization state for these proteins using purified native transporters isolated under mild conditions. In this study, we used immunoaffinity purification to isolate the native porcine SERT, proceeding to solve its cryo-EM structure in complex with the 15B8 Fab. Together with FSEC data, we show that nSERT is best described as a monomer rather than as a dimer or a multimer (Fig. 1-2). Previous biochemical studies suggested that transmembrane helix (TM) 11 and TM12 form oligomeric interfaces in hSERT, and also suggested potential contributions by TM5 and TM6 (ref.32). By contrast, the x-ray structure of SERT indicates that the kinked TM12 and the additional C-terminal helix protruding into the membrane preclude dimerization of SERT via a LeuT-like, TM12 interface[4]. Furthermore, subsequent structural studies revealed that TM5 and TM6 are directly involved in the transporter's conformational transitions between different functional states, and thus we speculate that their required flexibility is likely to incompatible with the formation of dimers or multimers. Thus, our findings provide support for monomeric SERT in its native environment. Nevertheless, our study does not exclude the possibility of dimeric or multimeric arrangements present in the native membrane, perhaps the loss of lipids, such as PIP2, during extraction with detergent results in an exclusively monomeric transporter. Thus, further studies are needed to address the roles that membrane constituents may play in oligomer formation.

Previous structural studies of dDAT complexed with methamphetamine, cocaine, or their analogs provided a structural framework for showing how addictive psychostimulants stabilize the transporter in an outward-open conformation[15]. Here, we

bioRxiv preprint doi: https://doi.org/10.1101/2022.09.03.506477; this version posted September 5, 2022. The copyright holder for this preprint (which was not certified by peer review) is the author/funder. All rights reserved. No reuse allowed without permission.

297 employed native SERT and single particle cryo-EM to study amphetamine and cocaine
298 binding. We find that compared to the corresponding dDAT structures,
299 methamphetamine and cocaine have similar binding site locations and interactions at
300 the central site of SERT. There are differences in the transporter conformations,
301 however, with cocaine inducing an outward-occluded conformation of SERT, caused
302 by Phe372 rotating 'inward', to cover the tropane ring of cocaine, thereby blocking the
303 release of the ligand from the central site, a conformational change not seen in the
304 transport inactive, cocaine-bound dDAT structures (Fig. 3).

305 CHOL is an important constituent of eukaryotic plasma membranes and
306 modulates the function of neurotransmitter transporters. It is required for optimal
307 reconstitution of the GABA transporter[66] and is implicated in the function of SERT[50]
308 via direct CHOL-protein interactions, as well as in the activity of DAT[57,61], NET[53,54],
309 and GlyT2[58]. In the case of SERT, CHOL modulates its functional properties by
310 enhancing substrate transport and antagonist binding[50]. MD simulations show that
311 CHOL molecules are embedded in multiple sites of SERT[63], three of which have been
312 confirmed by structural studies[8,10,15,64]. Here we discovered two CHOL binding sites in
313 nSERT. In addition, we also observed a non-protein density in the serotonin allosteric
314 site (Fig. 4). Although this region of TM10, TM11, and TM12 has been indicated to be
315 a potential CHOL-binding site, our MD simulations suggest that CHOL cannot stably
316 bind within this site. We instead find that DHA is well accommodated into the
317 experimental density, and is stably bound as determined by MD simulations and free
318 energy calculations. Conclusive determination of the native lipid molecules that bind to
319 the allosteric site, in addition to DHA, awaits further study.

320 Using biochemical analysis and cryo-EM, we observed under conditions of mild
321 non-ionic detergents, the native, mammalian nSERT is isolated as a monomeric species,
322 without interacting proteins, yet bound with multiple CHOL and lipid molecules.
323 Nevertheless, the data presented in this study do not completely exclude the possibility
324 of SERT oligomers in the native membrane. We investigated amphetamine and cocaine
325 binding to nSERT and discovered that both ligands occupy the central site, where they

bioRxiv preprint doi: https://doi.org/10.1101/2022.09.03.506477; this version posted September 5, 2022. The copyright holder for this preprint (which was not certified by peer review) is the author/funder. All rights reserved. No reuse allowed without permission.

326 are involved in numerous interactions with surrounding residues. Our studies of native
327 SERT, in complex with addictive drugs provides a strategy for the study of native
328 monoamine transporters. In summary, the nSERT complexes demonstrate the
329 mechanism of psychostimulant inhibition and shed light onto the modulation of NSSs
330 by illicit substances and the interactions of lipids with the transmembrane domain,
331 particularly within the allosteric binding site.

bioRxiv preprint doi: https://doi.org/10.1101/2022.09.03.506477; this version posted September 5, 2022. The copyright holder for this preprint (which was not certified by peer review) is the author/funder. All rights reserved. No reuse allowed without permission.

Methods

Antibody purification

The 15B8 Fab construct[8] was cloned into the pFastBac-dual vector, including a GP64 signal sequence. A mCherry tag, followed by a twin Strep [TrpSerHisProGlnPheGluLys(GlyGlyGlySer)2GlyGlySerAlaTrpSerHisProGlnPheGluLys] and a His_{10} purification tag, were fused to the C-terminus of the heavy chain. Baculovirus was prepared according to standard methods. The Sf9 cells were infected by the recombinant baculovirus at a cell density of 2×10^6 ml^{-1} at 27 °C. The culture supernatant was then collected 96 h after infection by centrifugation at 5,000 rpm for 20 min using a JLA 8.1000 rotor at 4 °C. The 15B8 Fab was purified from Sf9 supernatant by metal ion affinity chromatography followed by size exclusion chromatography.

Isolation of nSERT

One pig brain (~150 g) was homogenized with a Dounce homogenizer in ice-cold Tris-buffered saline buffer (TBS; 20 mM Tris-HCl, pH 8.0, 150 mM NaCl) supplemented with 1 mM PMSF, 0.8 µM aprotinin, 2 µg ml^{-1} leupeptin, and 2 µM pepstatin. The homogenized brain suspension was then sonicated using a sonicator equipped with a tip size of 1.27 cm, for 15 min with 3 s on and 5 s off, at medium power, on ice. The resulting solution was then clarified by centrifugation for 20 min at 10,000g at 4 °C, the supernatant was collected and applied for further centrifugation at 40,000 rpm for 1 h at 4 °C (45 Ti fixed-angle rotor, Beckman) to pellet the membranes. The membranes were resuspended in 40 ml ice-cold TBS and further homogenized with a Dounce homogenizer. The membranes were solubilized in 100 ml ice-cold TBS containing 20 mM n-dodecyl-β-D-maltoside (DDM) and 2.5 mM cholesteryl hemisuccinate (CHS) in the presence of 1 mg of 15B8 Fab, 100 µM methamphetamine or 10 µM cocaine, for 1 h at 4°C. The lysate was centrifuged at 40,000 rpm for 50 min at 4°C (45 Ti fixed-angle rotor, Beckman) and the transporter-Fab complex was isolated by affinity chromatography using Strep-Tactin resin. The complex was further purified

bioRxiv preprint doi: https://doi.org/10.1101/2022.09.03.506477; this version posted September 5, 2022. The copyright holder for this preprint (which was not certified by peer review) is the author/funder. All rights reserved. No reuse allowed without permission.

by fluorescence detection size exclusion chromatography (FSEC)[67] on a Superose 6 Increase 10/300 column in a buffer composed of 20 mM Tris-HCl (pH 8) supplemented with 100 mM NaCl, 1 mM DDM, 0.2 mM CHS, and 100 µM methamphetamine or 10 µM cocaine. The peak fraction containing the nSERT-Fab complexes was collected and used for biochemical and single particle cryo-EM analysis.

Western blot analysis

Purified nSERT was run on a SDS-PAGE gel and subsequently transferred to a nitrocellulose membrane. Antibodies used for detection were 10F2, a monoclonal antibody generated in house, and which can recognize the linear epitope of SERT. An IRDye 680RD anti-mouse secondary antibody (LI-COR), was used for visualization. Blots were developed from the secondary antibody at a ratio of 1:10,000 and imaged by Odyssey® DLx Imaging System.

Radioligand binding assay

A saturation binding experiment using [^{3}H]paroxetine was performed via the scintillation proximity assay (SPA)[68] using the lysate of pig brain membranes in SPA buffer (20 mM Tris-HCl, pH 8, 100 mM NaCl, 1 mM DDM, 0.2 mM CHS). The membrane lysates were mixed with Cu-YSi beads (0.5 mg ml^{-1}) in SPA buffer, and [^{3}H]paroxetine at a concentration of 0.3 to 40 nM. Nonspecific binding was estimated by experiments that included 100 µM cold S-citalopram. Data were analyzed using a single-site binding function.

Methamphetamine and cocaine competition binding experiments were performed using SPA with Cu-YSi beads (0.5 mg ml^{-1}) in SPA buffer. For the methamphetamine competition assays, SPA was performed with Strep-purified nSERT, 10 nM [^{3}H]paroxetine, and 1 µM to 100 mM cold methamphetamine. For the cocaine competition assays, SPA was done with Strep-purified nSERT and 10 nM [^{3}H]paroxetine in the presence of 1 nM to 1 mM cold cocaine. Experiments were performed in triplicate. The error bars for each data point represent the standard error of the mean (SEM). K_i values were determined with the Cheng-Prusoff equation[69] in

bioRxiv preprint doi: https://doi.org/10.1101/2022.09.03.506477; this version posted September 5, 2022. The copyright holder for this preprint (which was not certified by peer review) is the author/funder. All rights reserved. No reuse allowed without permission.

GraphPad Prism.

Cryo-EM sample preparation and data acquisition

The purified nSERT-15B8 Fab complex was concentrated to 0.1 mg ml^{-1}, after which either 10 mM methamphetamine or 1 mM cocaine, together with 100 μM fluorinated n-octyl-β-D-maltoside (final concentration) were added prior to grid preparation. A droplet of 2.5 μl of protein solution was applied to glow-discharged Quantifoil 200 or 300 mesh 2/1 or 1.2/1.3 gold grids covered by 2 nm of continuous carbon film. The grids were blotted for 2.0 s at 100% humidity at 20°C, followed by plunging into liquid ethane cooled by liquid nitrogen, using a Vitrobot Mark IV. The nSERT datasets were collected on a 300 kV FEI Titan Krios microscope located at the HHMI Janelia Research Campus, equipped with a K3 detector, at a nominal magnification of 105,000x, corresponding to a pixel size of 0.831 Å. The typical defocus values ranged from -1.0 to -2.5 μm. Each stack was exposed for 4.0 s and dose-fractionated into 60 frames, with a total dose of 60 e^{-} $Å^{-2}$. Images were recorded using the automated acquisition program SerialEM[70].

Cryo-EM image processing

The beam-induced motion was corrected by MotionCor2 (ref.71). The defocus values were estimated by Gctf[72] and particles were picked by blob-picker in cryoSPARC[73]. After two rounds of 2D classification, 2D classes with clear secondary structures were selected. An initial model was then generated by cryoSPARC. The initial model was further used for the following heterogeneous refinement. A round of 3D classification without image alignment was performed in RELION-3.1 (ref.74), with a soft mask excluding the constant domain of 15B8 Fab and micelle. The selected particles were imported back to cryoSPARC for homogeneous refinement, local contrast transfer function (CTF) refinement, and nonuniform refinement. The local resolution of the final map was estimated in cryoSPARC.

For the nSERT-15B8 Fab complex in the presence of (+)-methamphetamine, 7,794,907 particles were picked in cryoSPARC, which after rounds of 2D classification

bioRxiv preprint doi: https://doi.org/10.1101/2022.09.03.506477; this version posted September 5, 2022. The copyright holder for this preprint (which was not certified by peer review) is the author/funder. All rights reserved. No reuse allowed without permission.

and heterogeneous refinement, left 348,745 particles (binned to a 200-pixel box, 1.662 Å pixel^{-1}). Particles were reextracted (360-pixel box, 0.831 Å pixel^{-1}) and subjected for homogeneous refinement and nonuniform refinement in cryoSPARC, then subjected to 3D classification with 10 classes in RELION-3.1 without image alignment (360-pixel box, 0.831 Å pixel^{-1}). Particles from three classes with clear TM features were combined and subjected to homogeneous refinement, local CTF refinement, and nonuniform refinement in cryoSPARC, respectively (Supplementary Fig. 2).

For the nSERT-15B8 Fab complex with cocaine, a total of 7,560,137 particles were picked from 16,094 movies in cryoSPARC with a box size of 200 pixels (1.662 Å pixel^{-1}). After rounds of 2D classification and heterogeneous refinement, 338,343 particles were selected, re-extracted (400-pixel box, 0.831 Å pixel^{-1}), and subjected to homogeneous refinement, nonuniform refinement in cryoSPARC, and further subjected to 3D classification with 10 classes in RELION-3.1 without image alignment. Two well-resolved classes with 243,207 particles were combined and further refined in cryoSPARC with homogeneous refinement, local CTF refinement, and nonuniform refinement (Supplementary Fig. 3).

Model building and refinement

Interpretation of the cryo-EM maps exploited rigid-body fitting of the SERT-antibody complex models derived from previous cryo-EM studies. The outward-open ΔN72/C13 SERT-15B8 Fab complex with a 5-HT model (PDB code: 7LIA) was used as a reference. The initial model was generated via rigid-body fitting of the homology models to the density map in UCSF ChimeraX[75]. The model was then manually adjusted in Coot[76]. The model was further refined using real-space refinement in PHENIX[77]. Figures were prepared in UCSF ChimeraX.

System preparation for MD simulations

We performed molecular dynamics (MD) simulations of the cocaine-SERT complex in a hydrated lipid bilayer to explore the identity of the ligand in the allosteric site ligand. Triplicates of four simulation systems were studied, with the allosteric site

bioRxiv preprint doi: https://doi.org/10.1101/2022.09.03.506477; this version posted September 5, 2022. The copyright holder for this preprint (which was not certified by peer review) is the author/funder. All rights reserved. No reuse allowed without permission.

444 occupied by either docosahexaenoic acid (DHA) in charged or neutral forms (DHA^- or
445 DHA^0, respectively), cholesterol (CHOL), or cholesteryl hemisuccinate (CHS). The
446 initial coordinates of CHS and DHA^- were transferred from experimental modeling,
447 while CHOL was constructed into the CHS model, and DHA^0 was constructed by
448 protonating the DHA^- model using the PSFGEN plugin in VMD[78]. The missing side
449 chains and hydrogen atoms in the protein were added using the PSFGEN plugin in
450 VMD[78]. The co-crystalized antibody fragment was removed. All bound Na^+ and Cl^-
451 ions, the cocaine molecule, and the two CHOL molecules bound to transmembrane
452 helices were retained. The allosteric site residue Phe532 was converted to the
453 corresponding tyrosine in wildtype hSERT. Glu173 was modeled as a protonated side
454 chain according to pKa calculations using PROPKA 3.0 (ref. 79). A disulfide bond was
455 introduced between Cys237 and Cys246. Neutral N-terminal and C-terminal 'caps'
456 were added to the first and last residue of the protein segment, respectively. All protein
457 models were internally hydrated using the DOWSER plugin[80,81] of VMD and externally
458 solvated using the SOLVATE program[82]. The models were then oriented according to
459 the Orientations of Proteins in Membranes (OPM) database[83] and embedded in a lipid
460 bilayer composed of 218 1-palmitoyl-2-oleoyl-sn-glycero-3-phosphocholine (POPC)
461 and 94 CHOL molecules from CHARMM-GUI[84]. The systems were next solvated and
462 neutralized with a 150 mM NaCl aqueous solution in VMD[78], resulting in simulation
463 systems of ~160,000 atoms, with approximate dimensions of 112 Å × 112 Å × 120 Å
464 before equilibration. Each simulation system was replicated into three independent
465 copies with lipid distributions randomized by shuffling lipid molecules within each
466 leaflet using the VMD plugin Membrane Mixer[85].

467 **Equilibrium MD simulations**

468 All simulations were performed using NAMD2[86,87] and the CHARMM36m
469 force fields[87] for proteins, CHARMM36 force fields for lipids (including CHS, CHOL,
470 DHA^- and DHA^0)[88], and the TIP3P model for water[89], along with the NBFIX
471 modifications for non-bonded interactions[90,91]. The force field parameters for cocaine
472 were obtained from the CGenFF server[92]. All simulations were carried out as

bioRxiv preprint doi: https://doi.org/10.1101/2022.09.03.506477; this version posted September 5, 2022. The copyright holder for this preprint (which was not certified by peer review) is the author/funder. All rights reserved. No reuse allowed without permission.

473 isothermal-isobaric (NPT) ensembles under periodic boundary conditions and
474 simulated in a flexible cell, whose dimensions could change independently while
475 keeping a constant ratio in the xy (membrane) plane. A constant temperature of 310 K
476 was maintained using Langevin dynamics with a 1.0-ps^{-1} damping coefficient, and a
477 constant pressure of 1.01325 bar was maintained with the Langevin piston Nosé-
478 Hoover method[93]. Non-bonded interactions were calculated in a pairwise manner with
479 the 12-Å cut-off, and a switching function applied between 10 Å and 12 Å. Long-range,
480 non-bonded interactions were calculated with the particle mesh Ewald (PME) method[94].
481 Bond lengths involving hydrogen atoms were constrained using the SHAKE[95] and
482 SETTLE algorithms[96]. Simulations were integrated in 2-fs time steps, and trajectories
483 were recorded every 10 ps.

484 The four simulation systems, each replicated into three independent copies were
485 simulated following these steps: (1) 3,000 steps of energy minimization; (2) 15 ns of
486 MD equilibration, during which Cα atoms, non-hydrogen atoms of ligands, and all
487 bound ions were restrained by harmonic potentials with decreasing force constants (k
488 = 5, 2.5, 1 kcal mol^{-1} $Å^{-2}$ for 5 ns each) to allow for protein side chain relaxation and
489 protein hydration; (3) 150 ns production MD run, during which harmonic potentials (k
490 = 1 kcal mol^{-1} $Å^{-2}$ for 5 ns each) were applied to only Cα atoms to avoid undesired
491 protein conformational deviation but allowing free diffusion of the allosteric site ligand.

492 **Free energy characterization of ligand binding**

493 The bias-exchange umbrella sampling (BEUS) method[97] was employed to
494 characterize the binding energy profiles of CHOL and DHA^- to the allosteric site. The
495 ligand-TM1b/TM6a distance, measured as the center-of-mass distance between the
496 non-hydrogen atoms in the ligand and Cα atoms in the extracellular ends of TM1b and
497 TM6a (residues 145-148 and 361-364), was chosen as the reaction coordinate to sample
498 ligand binding. The initial distances for the modeled CHOL and DHA^- were 17.2 and
499 15.2 Å, respectively. We chose reaction coordinates ranging from 14 to 21.5 Å and 15
500 to 22.5 Å for CHOL and DHA^-, respectively, to sample ligands unbinding from the
501 allosteric site. Each reaction coordinate was divided into 16 windows with a spacing of

bioRxiv preprint doi: https://doi.org/10.1101/2022.09.03.506477; this version posted September 5, 2022. The copyright holder for this preprint (which was not certified by peer review) is the author/funder. All rights reserved. No reuse allowed without permission.

0.5 Å. The initial conformations in each window were captured from steered MD simulations using the COLVAR module[98] in NAMD, in which the ligand was pulled towards the desired distances using a harmonic potential (k = 10 kcal mol^{-1} $Å^{-2}$) moving at a 0.5 Å ns^{-1} rate. The BEUS simulations were performed for 60 ns in each window. The Hamiltonian replica exchange was attempted every 1 ps between neighboring windows. Weighted Histogram Analysis Method (WHAM)[99,100] was used to construct the free energy profiles and perform error analysis using the Monte Carlo bootstrapping method.

Data availability

The 3D cryo-EM density maps and molecular coordinates have been deposited in the Electron Microscopy Data Bank (EMDB) and Protein Data Bank (PDB) for the SERT-15B8-Fab-methamphetamine outward (EMD-27384; 8DE4) and SERT-15B8-Fab-cocaine outward-occluded (EMD-27383; 8DE3) reconstructions and structures, respectively.

Acknowledgments

We thank Rui Yan at the HHMI Janelia CryoEM Facility for help in microscope operation and data collection. A portion of this research was supported by NIH grant U24GM129547 and performed at the PNCC at OHSU and accessed through EMSL (grid.436923.9), a DOE Office of Science User Facility sponsored by the Office of Biological and Environmental Research. Simulations in this study have been performed using allocations at National Science Foundation Supercomputing Centers (XSEDE grant MCA06N060). This work was otherwise funded by the NIH (R01 MH070039 and P41 GM104601). E.G. is supported by Jennifer and Bernard LaCroute and is an investigator of the Howard Hughes Medical Institute.

Author contributions

D.Y. and E.G. designed the project. D.Y. performed all the experiments. D.Y. and E.G. wrote the manuscript. Z.Z. and E.T. performed molecular dynamics simulations, and

bioRxiv preprint doi: https://doi.org/10.1101/2022.09.03.506477; this version posted September 5, 2022. The copyright holder for this preprint (which was not certified by peer review) is the author/funder. All rights reserved. No reuse allowed without permission.

wrote sections related to computational methods. All authors contributed to editing and manuscript preparation.

Competing interests

The authors declare no competing interests.

bioRxiv preprint doi: https://doi.org/10.1101/2022.09.03.506477; this version posted September 5, 2022. The copyright holder for this preprint (which was not certified by peer review) is the author/funder. All rights reserved. No reuse allowed without permission.

References

1 Berger, M., Gray, J. A. & Roth, B. L. The expanded biology of serotonin. *Annu. Rev. Med.* **60**, 355-366, doi:10.1146/annurev.med.60.042307.110802 (2009).

2 Kristensen, A. S. *et al.* SLC6 neurotransmitter transporters: structure, function, and regulation. *Pharmacol. Rev.* **63**, 585-640, doi:10.1124/pr.108.000869 (2011).

3 Broer, S. & Gether, U. The solute carrier 6 family of transporters. *Br. J. Pharmacol.* **167**, 256-278, doi:10.1111/j.1476-5381.2012.01975.x (2012).

4 Yamashita, A., Singh, S. K., Kawate, T., Jin, Y. & Gouaux, E. Crystal structure of a bacterial homologue of Na+/Cl--dependent neurotransmitter transporters. *Nature* **437**, 215-223, doi:10.1038/nature03978 (2005).

5 Mitchell, P. A general theory of membrane transport from studies of bacteria. *Nature* **180**, 134-136, doi:10.1038/180134a0 (1957).

6 Penmatsa, A. & Gouaux, E. How LeuT shapes our understanding of the mechanisms of sodium-coupled neurotransmitter transporters. *J. Physiol.* **592**, 863-869, doi:10.1113/jphysiol.2013.259051 (2014).

7 Malinauskaite, L. *et al.* A mechanism for intracellular release of Na+ by neurotransmitter/sodium symporters. *Nat. Struct. Mol. Biol.* **21**, 1006-1012, doi:10.1038/nsmb.2894 (2014).

8 Coleman, J. A., Green, E. M. & Gouaux, E. X-ray structures and mechanism of the human serotonin transporter. *Nature* **532**, 334-339, doi:10.1038/nature17629 (2016).

9 Coleman, J. A. & Gouaux, E. Structural basis for recognition of diverse antidepressants by the human serotonin transporter. *Nat. Struct. Mol. Biol.* **25**, 170-175, doi:10.1038/s41594-018-0026-8 (2018).

10 Coleman, J. A. *et al.* Serotonin transporter-ibogaine complexes illuminate mechanisms of inhibition and transport. *Nature* **569**, 141-145, doi:10.1038/s41586-019-1135-1 (2019).

11 Coleman, J. A. *et al.* Chemical and structural investigation of the paroxetine-human serotonin transporter complex. *Elife* **9**, doi:10.7554/eLife.56427 (2020).

bioRxiv preprint doi: https://doi.org/10.1101/2022.09.03.506477; this version posted September 5, 2022. The copyright holder for this preprint (which was not certified by peer review) is the author/funder. All rights reserved. No reuse allowed without permission.

12 Shahsavar, A. *et al.* Structural insights into the inhibition of glycine reuptake. *Nature*, doi:10.1038/s41586-021-03274-z (2021).

13 Andersen, J., Kristensen, A. S., Bang-Andersen, B. & Stromgaard, K. Recent advances in the understanding of the interaction of antidepressant drugs with serotonin and norepinephrine transporters. *Chem. Commun. (Camb.)*, 3677-3692, doi:10.1039/b903035m (2009).

14 Howell, L. L. & Kimmel, H. L. Monoamine transporters and psychostimulant addiction. *Biochem. Pharmacol.* **75**, 196-217, doi:10.1016/j.bcp.2007.08.003 (2008).

15 Wang, K. H., Penmatsa, A. & Gouaux, E. Neurotransmitter and psychostimulant recognition by the dopamine transporter. *Nature* **521**, 322-327, doi:10.1038/nature14431 (2015).

16 Quick, M. W. Role of syntaxin 1A on serotonin transporter expression in developing thalamocortical neurons. *Int. J. Dev. Neurosci.* **20**, 219-224, doi:10.1016/s0736-5748(02)00021-7 (2002).

17 Chanrion, B. *et al.* Physical interaction between the serotonin transporter and neuronal nitric oxide synthase underlies reciprocal modulation of their activity. *Proc. Natl. Acad. Sci. U. S. A.* **104**, 8119-8124, doi:10.1073/pnas.0610964104 (2007).

18 Carneiro, A. M. & Blakely, R. D. Serotonin-, protein kinase C-, and Hic-5-associated redistribution of the platelet serotonin transporter. *J. Biol. Chem.* **281**, 24769-24780, doi:10.1074/jbc.M603877200 (2006).

19 Eriksen, J., Jorgensen, T. N. & Gether, U. Regulation of dopamine transporter function by protein-protein interactions: new discoveries and methodological challenges. *J. Neurochem.* **113**, 27-41, doi:10.1111/j.1471-4159.2010.06599.x (2010).

20 Rasmussen, T. N., Plenge, P., Bay, T., Egebjerg, J. & Gether, U. A single nucleotide polymorphism in the human serotonin transporter introduces a new site for N-linked glycosylation. *Neuropharmacology* **57**, 287-294, doi:10.1016/j.neuropharm.2009.05.009 (2009).

bioRxiv preprint doi: https://doi.org/10.1101/2022.09.03.506477; this version posted September 5, 2022. The copyright holder for this preprint (which was not certified by peer review) is the author/funder. All rights reserved. No reuse allowed without permission.

21 Blakely, R. D. *et al.* Regulated phosphorylation and trafficking of antidepressant-sensitive serotonin transporter proteins. *Biol. Psychiatry* **44**, 169-178, doi:10.1016/s0006-3223(98)00124-3 (1998).

22 Ramamoorthy, S., Samuvel, D. J., Buck, E. R., Rudnick, G. & Jayanthi, L. D. Phosphorylation of threonine residue 276 is required for acute regulation of serotonin transporter by cyclic GMP. *J. Biol. Chem.* **282**, 11639-11647, doi:10.1074/jbc.M611353200 (2007).

23 Zarpellon, A. *et al.* Serotonin (5-HT) transport in human platelets is modulated by Src-catalysed Tyr-phosphorylation of the plasma membrane transporter SERT. *Cell. Physiol. Biochem.* **21**, 87-94, doi:10.1159/000113750 (2008).

24 Sitte, H. H. & Freissmuth, M. Oligomer formation by Na+-Cl--coupled neurotransmitter transporters. *Eur. J. Pharmacol.* **479**, 229-236, doi:10.1016/j.ejphar.2003.08.072 (2003).

25 Sitte, H. H., Farhan, H. & Javitch, J. A. Sodium-dependent neurotransmitter transporters: oligomerization as a determinant of transporter function and trafficking. *Mol. Interv.* **4**, 38-47, doi:10.1124/mi.4.1.38 (2004).

26 Mellerup, E. T., Plenge, P. & Nielsen, M. Size determination of binding polymers for [3H]imipramine and [3H]paroxetine in human platelet membranes. *Eur. J. Pharmacol.* **106**, 411-413, doi:10.1016/0014-2999(84)90730-1 (1984).

27 Jess, U., Betz, H. & Schloss, P. The membrane-bound rat serotonin transporter, SERT1, is an oligomeric protein. *FEBS Lett.* **394**, 44-46, doi:10.1016/0014-5793(96)00916-7 (1996).

28 Kilic, F. & Rudnick, G. Oligomerization of serotonin transporter and its functional consequences. *Proc. Natl. Acad. Sci. U. S. A.* **97**, 3106-3111, doi:10.1073/pnas.060408997 (2000).

29 Kocabas, A. M., Rudnick, G. & Kilic, F. Functional consequences of homo- but not hetero-oligomerization between transporters for the biogenic amine neurotransmitters. *J. Neurochem.* **85**, 1513-1520, doi:10.1046/j.1471-4159.2003.01793.x (2003).

30 Torres, G. E. *et al.* Oligomerization and trafficking of the human dopamine

bioRxiv preprint doi: https://doi.org/10.1101/2022.09.03.506477; this version posted September 5, 2022. The copyright holder for this preprint (which was not certified by peer review) is the author/funder. All rights reserved. No reuse allowed without permission.

transporter. Mutational analysis identifies critical domains important for the functional expression of the transporter. *J. Biol. Chem.* **278**, 2731-2739, doi:10.1074/jbc.M201926200 (2003).

31 Schmid, J. A. *et al.* Oligomerization of the human serotonin transporter and of the rat GABA transporter 1 visualized by fluorescence resonance energy transfer microscopy in living cells. *J. Biol. Chem.* **276**, 3805-3810, doi:10.1074/jbc.M007357200 (2001).

32 Just, H., Sitte, H. H., Schmid, J. A., Freissmuth, M. & Kudlacek, O. Identification of an additional interaction domain in transmembrane domains 11 and 12 that supports oligomer formation in the human serotonin transporter. *J. Biol. Chem.* **279**, 6650-6657, doi:10.1074/jbc.M306092200 (2004).

33 Bartholomaus, I. *et al.* Glycine transporter dimers: evidence for occurrence in the plasma membrane. *J. Biol. Chem.* **283**, 10978-10991, doi:10.1074/jbc.M800622200 (2008).

34 Chen, N. & Reith, M. E. Substrates dissociate dopamine transporter oligomers. *J. Neurochem.* **105**, 910-920, doi:10.1111/j.1471-4159.2007.05195.x (2008).

35 Fjorback, A. W. *et al.* Serotonin transporter oligomerization documented in RN46A cells and neurons by sensitized acceptor emission FRET and fluorescence lifetime imaging microscopy. *Biochem. Biophys. Res. Commun.* **380**, 724-728, doi:10.1016/j.bbrc.2009.01.128 (2009).

36 Li, Y., Cheng, S. Y., Chen, N. & Reith, M. E. Interrelation of dopamine transporter oligomerization and surface presence as studied with mutant transporter proteins and amphetamine. *J. Neurochem.* **114**, 873-885, doi:10.1111/j.1471-4159.2010.06818.x (2010).

37 Hastrup, H., Karlin, A. & Javitch, J. A. Symmetrical dimer of the human dopamine transporter revealed by cross-linking Cys-306 at the extracellular end of the sixth transmembrane segment. *Proc. Natl. Acad. Sci. U. S. A.* **98**, 10055-10060, doi:10.1073/pnas.181344298 (2001).

38 Hastrup, H., Sen, N. & Javitch, J. A. The human dopamine transporter forms a tetramer in the plasma membrane: cross-linking of a cysteine in the fourth

bioRxiv preprint doi: https://doi.org/10.1101/2022.09.03.506477; this version posted September 5, 2022. The copyright holder for this preprint (which was not certified by peer review) is the author/funder. All rights reserved. No reuse allowed without permission.

transmembrane segment is sensitive to cocaine analogs. *J. Biol. Chem.* **278**, 45045-45048, doi:10.1074/jbc.C300349200 (2003).

39 Horiuchi, M. *et al.* Surface-localized glycine transporters 1 and 2 function as monomeric proteins in Xenopus oocytes. *Proc. Natl. Acad. Sci. U. S. A.* **98**, 1448-1453, doi:10.1073/pnas.041329498 (2001).

40 Jayaraman, K. *et al.* Dopamine transporter oligomerization involves the scaffold domain, but spares the bundle domain. *PLoS Comput. Biol.* **14**, e1006229, doi:10.1371/journal.pcbi.1006229 (2018).

41 Anderluh, A. *et al.* Direct PIP2 binding mediates stable oligomer formation of the serotonin transporter. *Nat Commun* **8**, 14089, doi:10.1038/ncomms14089 (2017).

42 Baucum, A. J., 2nd, Rau, K. S., Riddle, E. L., Hanson, G. R. & Fleckenstein, A. E. Methamphetamine increases dopamine transporter higher molecular weight complex formation via a dopamine- and hyperthermia-associated mechanism. *J. Neurosci.* **24**, 3436-3443, doi:10.1523/JNEUROSCI.0387-04.2004 (2004).

43 Siciliano, C. A. *et al.* Amphetamine Reverses Escalated Cocaine Intake via Restoration of Dopamine Transporter Conformation. *J. Neurosci.* **38**, 484-497, doi:10.1523/JNEUROSCI.2604-17.2017 (2018).

44 Javanainen, M., Martinez-Seara, H. & Vattulainen, I. Excessive aggregation of membrane proteins in the Martini model. *PLoS One* **12**, e0187936, doi:10.1371/journal.pone.0187936 (2017).

45 Periole, X., Zeppelin, T. & Schiott, B. Dimer Interface of the Human Serotonin Transporter and Effect of the Membrane Composition. *Sci. Rep.* **8**, 5080, doi:10.1038/s41598-018-22912-7 (2018).

46 Lee, S. C. *et al.* A method for detergent-free isolation of membrane proteins in their local lipid environment. *Nat. Protoc.* **11**, 1149-1162, doi:10.1038/nprot.2016.070 (2016).

47 Tribet, C., Audebert, R. & Popot, J. L. Amphipols: polymers that keep membrane proteins soluble in aqueous solutions. *Proc. Natl. Acad. Sci. U. S. A.* **93**, 15047-15050, doi:10.1073/pnas.93.26.15047 (1996).

bioRxiv preprint doi: https://doi.org/10.1101/2022.09.03.506477; this version posted September 5, 2022. The copyright holder for this preprint (which was not certified by peer review) is the author/funder. All rights reserved. No reuse allowed without permission.

48 Docherty, J. R. & Alsufyani, H. A. Pharmacology of Drugs Used as Stimulants. *J. Clin. Pharmacol.* **61 Suppl 2**, S53-S69, doi:10.1002/jcph.1918 (2021).

49 Yang, D. & Gouaux, E. Illumination of serotonin transporter mechanism and role of the allosteric site. *Sci Adv* **7**, eabl3857, doi:10.1126/sciadv.abl3857 (2021).

50 Laursen, L. *et al.* Cholesterol binding to a conserved site modulates the conformation, pharmacology, and transport kinetics of the human serotonin transporter. *J. Biol. Chem.* **293**, 3510-3523, doi:10.1074/jbc.M117.809046 (2018).

51 Magnani, F., Tate, C. G., Wynne, S., Williams, C. & Haase, J. Partitioning of the serotonin transporter into lipid microdomains modulates transport of serotonin. *J. Biol. Chem.* **279**, 38770-38778, doi:10.1074/jbc.M400831200 (2004).

52 Scanlon, S. M., Williams, D. C. & Schloss, P. Membrane cholesterol modulates serotonin transporter activity. *Biochemistry* **40**, 10507-10513, doi:10.1021/bi010730z (2001).

53 Jayanthi, L. D., Samuvel, D. J. & Ramamoorthy, S. Regulated internalization and phosphorylation of the native norepinephrine transporter in response to phorbol esters. Evidence for localization in lipid rafts and lipid raft-mediated internalization. *J. Biol. Chem.* **279**, 19315-19326, doi:10.1074/jbc.M311172200 (2004).

54 Arapulisamy, O., Mannangatti, P. & Jayanthi, L. D. Regulated norepinephrine transporter interaction with the neurokinin-1 receptor establishes transporter subcellular localization. *J. Biol. Chem.* **288**, 28599-28610, doi:10.1074/jbc.M113.472878 (2013).

55 Adkins, E. M. *et al.* Membrane mobility and microdomain association of the dopamine transporter studied with fluorescence correlation spectroscopy and fluorescence recovery after photobleaching. *Biochemistry* **46**, 10484-10497, doi:10.1021/bi700429z (2007).

56 Foster, J. D., Adkins, S. D., Lever, J. R. & Vaughan, R. A. Phorbol ester induced

bioRxiv preprint doi: https://doi.org/10.1101/2022.09.03.506477; this version posted September 5, 2022. The copyright holder for this preprint (which was not certified by peer review) is the author/funder. All rights reserved. No reuse allowed without permission.

trafficking-independent regulation and enhanced phosphorylation of the dopamine transporter associated with membrane rafts and cholesterol. *J. Neurochem.* **105**, 1683-1699, doi:10.1111/j.1471-4159.2008.05262.x (2008).

57 Hong, W. C. & Amara, S. G. Membrane cholesterol modulates the outward facing conformation of the dopamine transporter and alters cocaine binding. *J. Biol. Chem.* **285**, 32616-32626, doi:10.1074/jbc.M110.150565 (2010).

58 Nunez, E., Alonso-Torres, P., Fornes, A., Aragon, C. & Lopez-Corcuera, B. The neuronal glycine transporter GLYT2 associates with membrane rafts: functional modulation by lipid environment. *J. Neurochem.* **105**, 2080-2090, doi:10.1111/j.1471-4159.2008.05292.x (2008).

59 Liu, X., Mitrovic, A. D. & Vandenberg, R. J. Glycine transporter 1 associates with cholesterol-rich membrane raft microdomains. *Biochem. Biophys. Res. Commun.* **384**, 530-534, doi:10.1016/j.bbrc.2009.05.014 (2009).

60 Butchbach, M. E., Tian, G., Guo, H. & Lin, C. L. Association of excitatory amino acid transporters, especially EAAT2, with cholesterol-rich lipid raft microdomains: importance for excitatory amino acid transporter localization and function. *J. Biol. Chem.* **279**, 34388-34396, doi:10.1074/jbc.M403938200 (2004).

61 Jones, K. T., Zhen, J. & Reith, M. E. Importance of cholesterol in dopamine transporter function. *J. Neurochem.* **123**, 700-715, doi:10.1111/jnc.12007 (2012).

62 Deveau, C. M., Rodriguez, E., Schroering, A. & Yamamoto, B. K. Serotonin transporter regulation by cholesterol-independent lipid signaling. *Biochem. Pharmacol.* **183**, 114349, doi:10.1016/j.bcp.2020.114349 (2021).

63 Ferraro, M., Masetti, M., Recanatini, M., Cavalli, A. & Bottegoni, G. Mapping Cholesterol Interaction Sites on Serotonin Transporter through Coarse-Grained Molecular Dynamics. *PLoS One* **11**, e0166196, doi:10.1371/journal.pone.0166196 (2016).

64 Penmatsa, A., Wang, K. H. & Gouaux, E. X-ray structure of dopamine transporter elucidates antidepressant mechanism. *Nature* **503**, 85-90,

bioRxiv preprint doi: https://doi.org/10.1101/2022.09.03.506477; this version posted September 5, 2022. The copyright holder for this preprint (which was not certified by peer review) is the author/funder. All rights reserved. No reuse allowed without permission.

743 doi:10.1038/nature12533 (2013).

744 65 Plenge, P., Yang D.Y., Salomon K., Laursen, L., Newman, A.H., Gouaux, E.,
745 Coleman, J.A., Loland, C.J. The antidepressant drug vilazodone is an allosteric
746 inhibitor of the serotonin transporter. . *Nat. Commun.* **12, 5063** (2021).

747 66 Shouffani, A., IKanner, B. Cholesterol is required for the reconstruction of the
748 sodium- and chloride-coupled, gamma-aminobutyric acid transporter from rat
749 brain. *J. Biol. Chem.* **265** (1990).

750 67 Kawate, T. & Gouaux, E. Fluorescence-detection size-exclusion
751 chromatography for precrystallization screening of integral membrane proteins.
752 *Structure* **14**, 673-681, doi:10.1016/j.str.2006.01.013 (2006).

753 68 Cook, N., Harris, A., Hopkins, A. & Hughes, K. Scintillation proximity assay
754 (SPA) technology to study biomolecular interactions. *Curr Protoc Protein Sci*
755 **Chapter 19**, Unit 19 18, doi:10.1002/0471140864.ps1908s27 (2002).

756 69 Cheng, Y. & Prusoff, W. H. Relationship between the inhibition constant (K1)
757 and the concentration of inhibitor which causes 50 per cent inhibition (I50) of
758 an enzymatic reaction. *Biochem. Pharmacol.* **22**, 3099-3108 (1973).

759 70 Mastronarde, D. N. Automated electron microscope tomography using robust
760 prediction of specimen movements. *J. Struct. Biol.* **152**, 36-51,
761 doi:10.1016/j.jsb.2005.07.007 (2005).

762 71 Zheng, S. Q. *et al.* MotionCor2: anisotropic correction of beam-induced motion
763 for improved cryo-electron microscopy. *Nat. Methods* **14**, 331-332,
764 doi:10.1038/nmeth.4193 (2017).

765 72 Zhang, K. Gctf: Real-time CTF determination and correction. *J. Struct. Biol.*
766 **193**, 1-12, doi:10.1016/j.jsb.2015.11.003 (2016).

767 73 Punjani, A., Rubinstein, J. L., Fleet, D. J. & Brubaker, M. A. cryoSPARC:
768 algorithms for rapid unsupervised cryo-EM structure determination. *Nat.*
769 *Methods* **14**, 290-296, doi:10.1038/nmeth.4169 (2017).

770 74 Scheres, S. H. RELION: implementation of a Bayesian approach to cryo-EM
771 structure determination. *J. Struct. Biol.* **180**, 519-530,
772 doi:10.1016/j.jsb.2012.09.006 (2012).

bioRxiv preprint doi: https://doi.org/10.1101/2022.09.03.506477; this version posted September 5, 2022. The copyright holder for this preprint (which was not certified by peer review) is the author/funder. All rights reserved. No reuse allowed without permission.

75 Pettersen, E. F. *et al.* UCSF ChimeraX: Structure visualization for researchers, educators, and developers. *Protein Sci.* **30**, 70-82, doi:10.1002/pro.3943 (2021).

76 Emsley, P. & Cowtan, K. Coot: model-building tools for molecular graphics. *Acta Crystallogr. D Biol. Crystallogr.* **60**, 2126-2132, doi:10.1107/S0907444904019158 (2004).

77 Adams, P. D. *et al.* PHENIX: a comprehensive Python-based system for macromolecular structure solution. *Acta Crystallogr. D Biol. Crystallogr.* **66**, 213-221, doi:10.1107/S0907444909052925 (2010).

78 Humphrey, W., Dalke, A. & Schulten, K. VMD: visual molecular dynamics. *J. Mol. Graph.* **14**, 33-38, 27-38, doi:10.1016/0263-7855(96)00018-5 (1996).

79 Olsson, M. H., Sondergaard, C. R., Rostkowski, M. & Jensen, J. H. PROPKA3: Consistent Treatment of Internal and Surface Residues in Empirical pKa Predictions. *J. Chem. Theory Comput.* **7**, 525-537, doi:10.1021/ct100578z (2011).

80 Zhang, L. & Hermans, J. Hydrophilicity of cavities in proteins. *Proteins* **24**, 433-438, doi:10.1002/(SICI)1097-0134(199604)24:4<433::AID-PROT3>3.0.CO;2-F (1996).

81 Gumbart, J., Trabuco, L. G., Schreiner, E., Villa, E. & Schulten, K. Regulation of the protein-conducting channel by a bound ribosome. *Structure* **17**, 1453-1464, doi:10.1016/j.str.2009.09.010 (2009).

82 Helmut Grubmüller. Solvate 1 .0, 1996. https://www.mpinat.mpg.de/grubmueller/solvate.

83 Lomize, M. A., Pogozheva, I. D., Joo, H., Mosberg, H. I. & Lomize, A. L. OPM database and PPM web server: resources for positioning of proteins in membranes. *Nucleic Acids Res.* **40**, D370-376, doi:10.1093/nar/gkr703 (2012).

84 Jo, S., Kim, T., Iyer, V. G. & Im, W. CHARMM-GUI: a web-based graphical user interface for CHARMM. *J. Comput. Chem.* **29**, 1859-1865, doi:10.1002/jcc.20945 (2008).

85 Licari, G., Dehghani-Ghahnaviyeh, S. & Tajkhorshid, E. Membrane Mixer: A Toolkit for Efficient Shuffling of Lipids in Heterogeneous Biological

bioRxiv preprint doi: https://doi.org/10.1101/2022.09.03.506477; this version posted September 5, 2022. The copyright holder for this preprint (which was not certified by peer review) is the author/funder. All rights reserved. No reuse allowed without permission.

Membranes. *J. Chem. Inf. Model.* **62**, 986-996, doi:10.1021/acs.jcim.1c01388 (2022).

86 Phillips, J. C. *et al.* Scalable molecular dynamics with NAMD. *J. Comput. Chem.* **26**, 1781-1802, doi:10.1002/jcc.20289 (2005).

87 Huang, J. *et al.* CHARMM36m: an improved force field for folded and intrinsically disordered proteins. *Nat. Methods* **14**, 71-73, doi:10.1038/nmeth.4067 (2017).

88 Klauda, J. B. *et al.* Update of the CHARMM all-atom additive force field for lipids: validation on six lipid types. *J. Phys. Chem. B* **114**, 7830-7843, doi:10.1021/jp101759q (2010).

89 Jorgensen, W. L. C., J.; Madura, D.;. Comparison of simple potential functions for simulating liquid water. *J. Chem. Phys* **79**, doi:https://doi.org/10.1063/1.445869 (1983).

90 Yoo, J. A., A.;. Improved Parametrization of Li+, Na+, K+, and Mg2+ Ions for All-Atom Molecular Dynamics Simulations of Nucleic Acid Systems. *J. Phys. Chem. Lett.* **3**, 45-50 (2011).

91 Yoo, J. & Aksimentiev, A. New tricks for old dogs: improving the accuracy of biomolecular force fields by pair-specific corrections to non-bonded interactions. *Phys. Chem. Chem. Phys.* **20**, 8432-8449, doi:10.1039/C7CP08185E (2018).

92 Vanommeslaeghe, K. *et al.* CHARMM general force field: A force field for drug-like molecules compatible with the CHARMM all-atom additive biological force fields. *J. Comput. Chem.* **31**, 671-690, doi:10.1002/jcc.21367 (2010).

93 Martyna, G. J. Constant pressure molecular dynamics algorithms. *J. Chem. Phys.* **101**, 4177, doi:https://doi.org/10.1063/1.467468 (1994).

94 Darden, T. Y., D.; Pedersen, L.； . Particle mesh Ewald: An N·log(N) method for Ewald sums in large systems. *J. Chem. Phys.* **98**, doi:https://doi.org/10.1063/1.464397 (1993).

bioRxiv preprint doi: https://doi.org/10.1101/2022.09.03.506477; this version posted September 5, 2022. The copyright holder for this preprint (which was not certified by peer review) is the author/funder. All rights reserved. No reuse allowed without permission.

95 Ryckaert, J. P. C., G.; Berendsen, H.J.C；. Numerical integration of the cartesian equations of motion of a system with constraints: molecular dynamics of n-alkanes. *Journal of Computational Physics* **23**, 327-341, doi:https://doi.org/10.1016/0021-9991(77)90098-5 (1977).

96 Miyamoto, S. K., P. A.;. Settle: An analytical version of the SHAKE and RATTLE algorithm for rigid water models. *Journal of Computational Chemistry* **13**, 952-962, doi: https://doi.org/10.1002/jcc.540130805 (1992).

97 Sugita, Y. Multidimensional replica-exchange method for free-energy calculations. *J. Chem. Phys.* **113**, doi:https://doi.org/10.1063/1.1308516 (2000).

98 Fiorin, G. K., M. L.; Hénin, J. Using collective variables to drive molecular dynamics simulations. *Mol. Phys.* **111**, doi:https://doi.org/10.1080/00268976.2013.813594 (2013).

99 Kumar, S. R., J. M.; Bouzida, D.; Swendsen, R. H.; Kollman, P. A. THE weighted histogram analysis method for free-energy calculations on biomolecules. I. The method. *J. Comput. Chem.* **13**, 1011-1021, doi: https://doi.org/10.1002/jcc.540130812 (1992).

100 Grossfield, Alan, "WHAM: the weighted histogram analysis method", version 2.1.11, http://membrane.urmc.rochester.edu/wordpress/?page_id=126.

bioRxiv preprint doi: https://doi.org/10.1101/2022.09.03.506477; this version posted September 5, 2022. The copyright holder for this preprint (which was not certified by peer review) is the author/funder. All rights reserved. No reuse allowed without permission.

Figure legends

Fig. 1 Purification and biochemical analysis of native SERT (nSERT). a Flow chart for nSERT purification. **b** FSEC profiles for screening of solubilization conditions. **c** Representative FSEC profile for nSERT in complex with the 15B8 Fab. **d** Western blot analysis of isolated nSERT after FSEC. The experiments were repeated two times with similar results. **e** Saturation binding of [^{3}H] paroxetine to nSERT. **f** Competition binding of (+)-methamphetamine with [^{3}H]paroxetine for nSERT. Symbols show the mean values derived from n=3 technical replicates. Error bars show the SEM. **g** Plots of competition binding of cocaine against [^{3}H]paroxetine for nSERT. Data are means ± SEM.

Fig. 2 The cryo-EM structure of nSERT in complex with (+)-methamphetamine or cocaine, respectively. a Overall structure of the (+)-methamphetamine complex in the outward-open conformation, shown in cartoon representation. **b** Cartoon representation of the cocaine complex in the outward-occluded conformation. (+)-methamphetamine, cocaine, cholesteryl hemisuccinate (CHS), and docosahexaenoic acid (DHA) are shown in space-filling representations.

Fig. 3 Ligands occupy the central site. a Close-up view of (+)-methamphetamine in the binding pocket with hydrogen bonds shown as dashed lines. **b** Slice view of nSERT in complex with (+)-methamphetamine. **c** Cocaine interactions within the central binding site. A hydrogen bond between cocaine and D135 is indicated with a dashed line. **d** Slab views of the extracellular cavity of nSERT in complex with cocaine.

Fig. 4 Cholesteryl hemisuccinate (CHS) and docosahexaenoic acid (DHA) binding in SERT. **a** and **d** Close-up views of CHS modeled at the junction of TM1, TM5, and TM7 interacting with multiple hydrophobic residues. **b** and **e**, CHS modeled at the junction of TM2, TM7, and TM11. **c** and **f**, DHA modeled at the allosteric site. **g** Time series of displacements of ligands modeled at the allosteric site during the MD simulation. DHA^-, DHA^0, CHOL, and CHS trajectories are plotted in green, purple, blue, and orange, respectively, and are shown for three independent simulations in each

bioRxiv preprint doi: https://doi.org/10.1101/2022.09.03.506477; this version posted September 5, 2022. The copyright holder for this preprint (which was not certified by peer review) is the author/funder. All rights reserved. No reuse allowed without permission.

878 case. Plots are smoothed using a sliding window of 1 ns. **h** Free energy profiles of DHA^-
879 and CHOL binding to the allosteric site along the ligand-TM1b/TM6a distance, with
880 molecular images showing DHA^- in the allosteric site (left) or dissociated into the
881 membrane (middle). The ligand-TM1b/TM6a distance is measured as the center-of-
882 mass distance between heavy atoms in the ligand (shown in VDW representation) and
883 Cα atoms from TM1b and TM6a (residues 145-148 and 361-364, shown as pink
884 spheres).

bioRxiv preprint doi: https://doi.org/10.1101/2022.09.03.506477; this version posted September 5, 2022. The copyright holder for this preprint (which was not certified by peer review) is the author/funder. All rights reserved. No reuse allowed without permission.

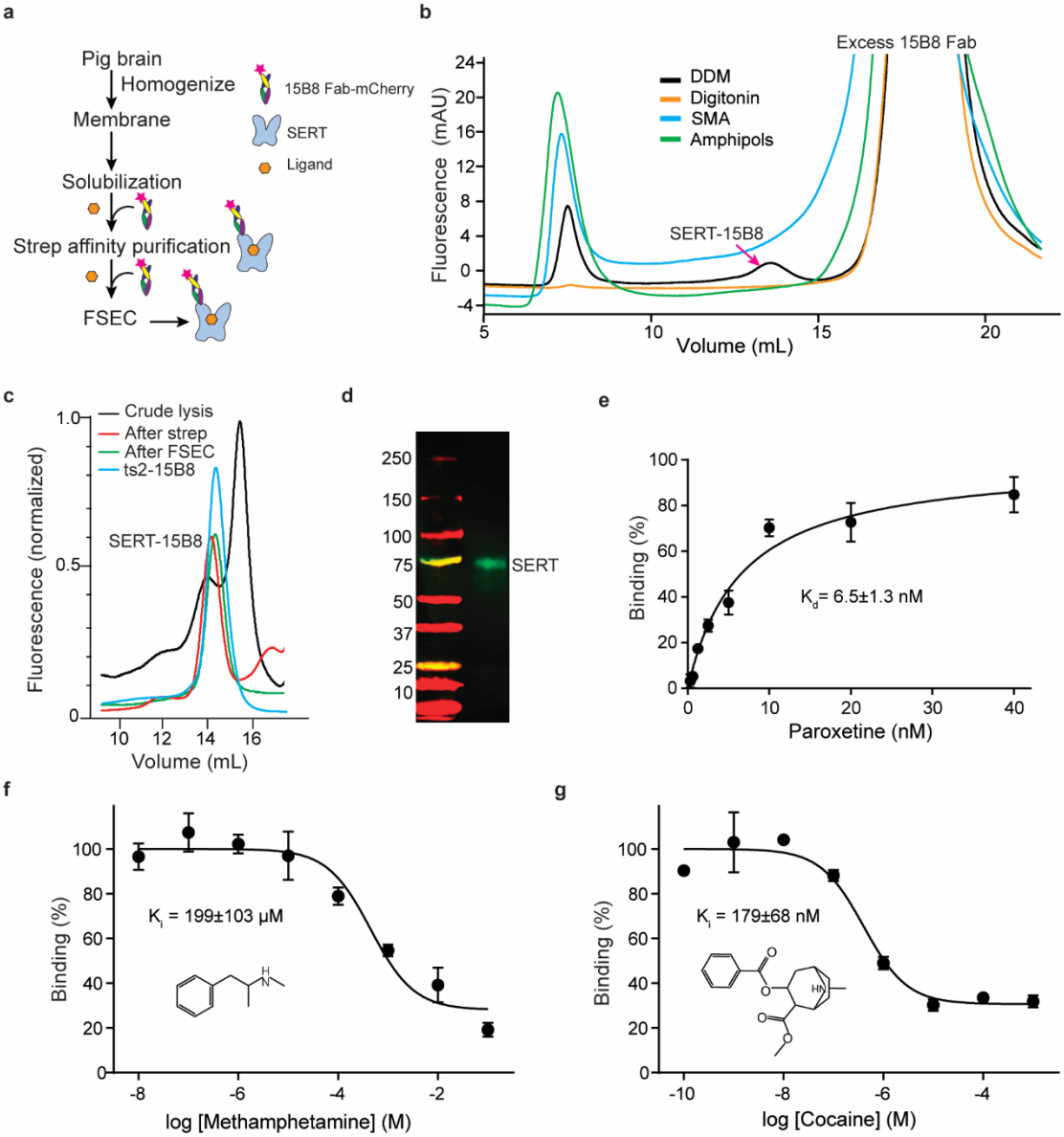

886 **Fig. 1 Purification and biochemical analysis of native SERT (nSERT). a** Flow chart
887 for nSERT purification. **b** FSEC profiles for screening of solubilization conditions. **c**
888 Representative FSEC profile for nSERT in complex with the 15B8 Fab. **d** Western blot
889 analysis of isolated nSERT after FSEC. The experiments were repeated two times with
890 similar results. **e** Saturation binding of [^{3}H] paroxetine to nSERT. **f** Competition binding
891 of (+)-methamphetamine with [^{3}H]paroxetine for nSERT. Symbols show the mean
892 values derived from n = 3 technical replicates. Error bars show the SEM. **g** Plots of
893 competition binding of cocaine against [^{3}H]paroxetine for nSERT. Data are means ±
894 SEM.

bioRxiv preprint doi: https://doi.org/10.1101/2022.09.03.506477; this version posted September 5, 2022. The copyright holder for this preprint (which was not certified by peer review) is the author/funder. All rights reserved. No reuse allowed without permission.

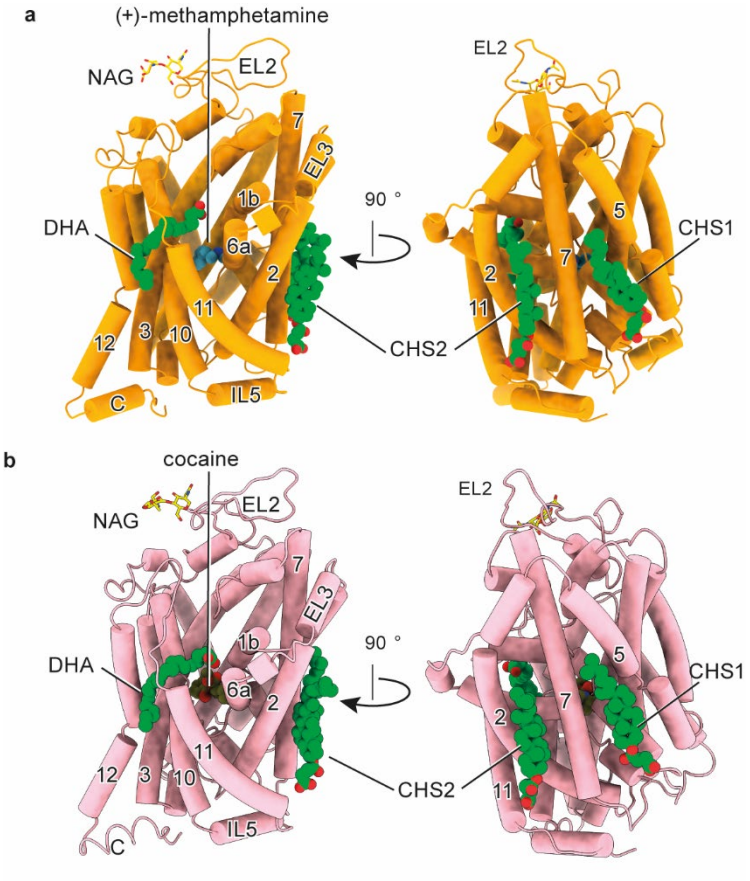

Fig. 2 The cryo-EM structure of nSERT in complex with (+)-methamphetamine or cocaine, respectively. a Overall structure of the (+)-methamphetamine complex in the outward-open conformation, shown in cartoon representation. **b** Cartoon representation of the cocaine complex in the outward-occluded conformation. (+)-methamphetamine, cocaine, cholesteryl hemisuccinate (CHS), and docosahexaenoic acid (DHA) are shown in space-filling representations.

bioRxiv preprint doi: https://doi.org/10.1101/2022.09.03.506477; this version posted September 5, 2022. The copyright holder for this preprint (which was not certified by peer review) is the author/funder. All rights reserved. No reuse allowed without permission.

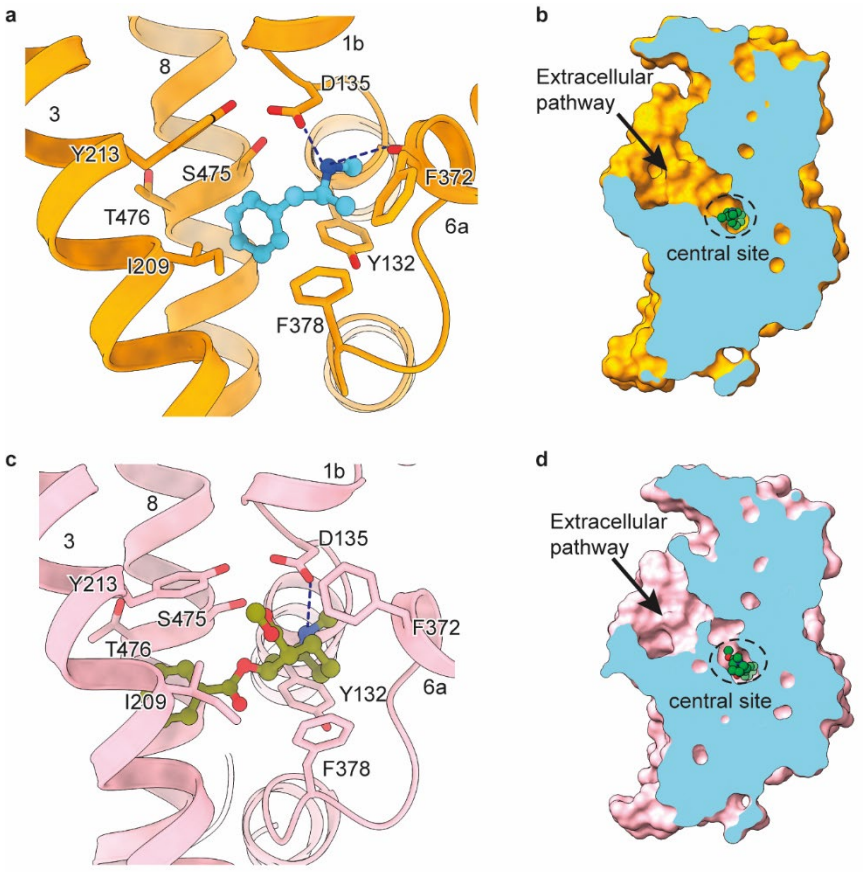

Fig. 3 Ligands occupy the central site. a Close-up view of (+)-methamphetamine in the binding pocket with hydrogen bonds shown as dashed lines. **b** Slice view of nSERT in complex with (+)-methamphetamine. **c** Cocaine interactions within the central binding site. A hydrogen bond between cocaine and D135 is indicated with a dashed line. **d** Slab views of the extracellular cavity of nSERT in complex with cocaine.

bioRxiv preprint doi: https://doi.org/10.1101/2022.09.03.506477; this version posted September 5, 2022. The copyright holder for this preprint (which was not certified by peer review) is the author/funder. All rights reserved. No reuse allowed without permission.

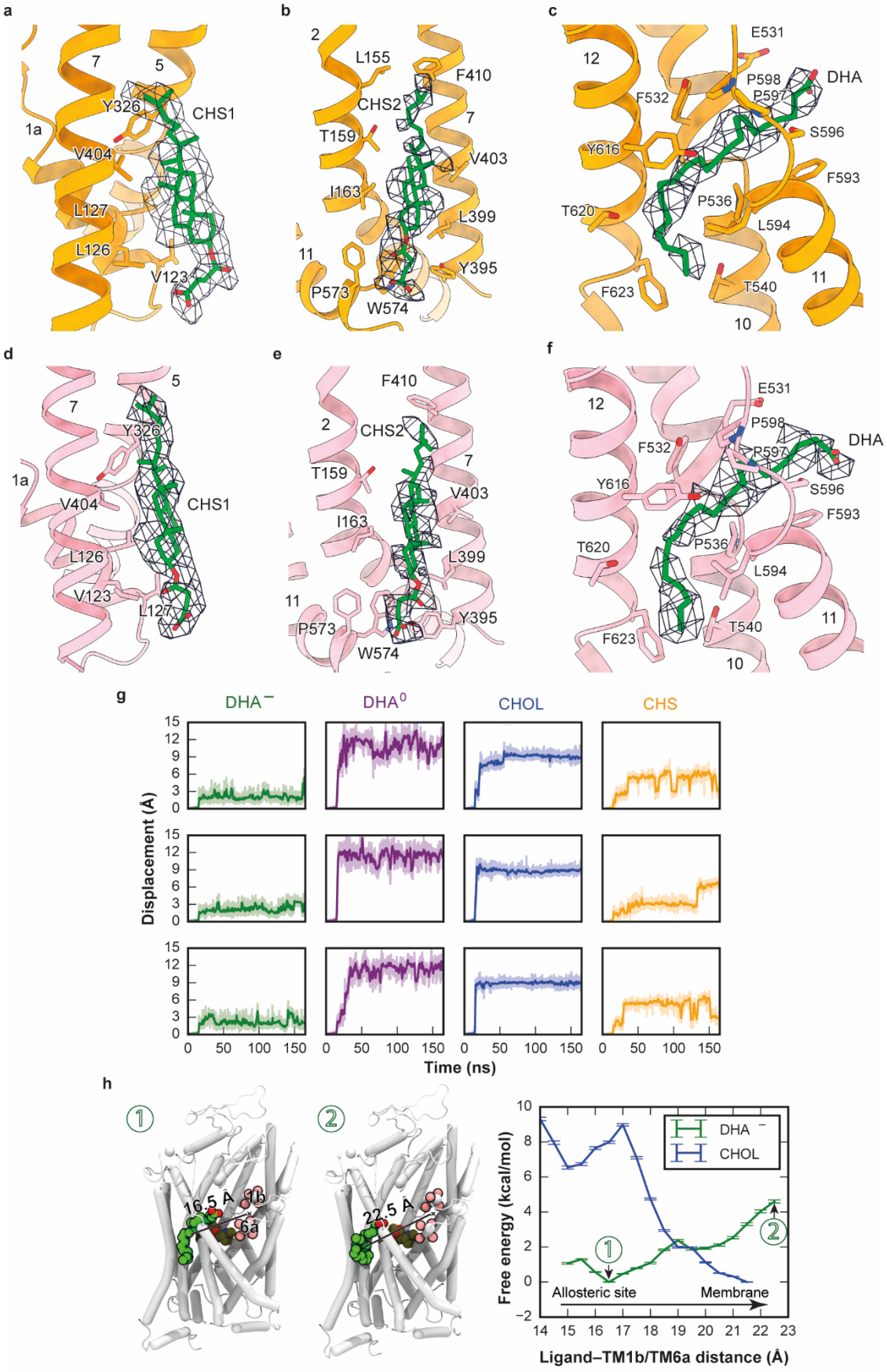

909 **Fig. 4 Cholesteryl hemisuccinate (CHS) and docosahexaenoic acid (DHA) binding**

bioRxiv preprint doi: https://doi.org/10.1101/2022.09.03.506477; this version posted September 5, 2022. The copyright holder for this preprint (which was not certified by peer review) is the author/funder. All rights reserved. No reuse allowed without permission.

910 **in SERT**. **a** and **d** Close-up views of CHS modeled at the junction of TM1, TM5, and
911 TM7 interacting with multiple hydrophobic residues. **b** and **e**, CHS modeled at the
912 junction of TM2, TM7, and TM11. **c** and **f**, DHA modeled at the allosteric site. **g** Time
913 series of displacements of ligands modeled at the allosteric site during the MD
914 simulation. DHA^{-}, DHA^{0}, CHOL, and CHS trajectories are plotted in green, purple,
915 blue, and orange, respectively, and are shown for three independent simulations in each
916 case. Plots are smoothed using a sliding window of 1 ns. **h** Free energy profiles of DHA^{-}
917 and CHOL binding to the allosteric site along the ligand–TM1b/TM6a distance, with
918 molecular images showing DHA^{-} in the allosteric site (left) or dissociated into the
919 membrane (middle). The ligand–TM1b/TM6a distance is measured as the center-of-
920 mass distance between heavy atoms in the ligand (shown in VDW representation) and
921 Cα atoms from TM1b and TM6a (residues 145–148 and 361–364, shown as pink
922 spheres).